On the application of instantaneous normal mode analysis to long time dynamics of liquids

G. V. Vijayadamodar and Abraham Nitzan
School of Chemistry, Tel Aviv University, Tel Aviv, 69978 Israel

(Received 14 February 1995; accepted 3 May 1995)

While the applicability of instantaneous normal mode (INM) analysis of liquids to short time dynamics is in principle obvious, its relevance to long time dynamics is not clear. Recent attempts by Keyes and co-workers to apply information obtained from this analysis to self-diffusion in supercooled liquid argon is critically analyzed. By extending the range of frequencies studied we show that both imaginary and real branches of the density of modes are represented better, for large ω, by $\ln[\rho(\omega)]\sim\omega^2/T$ than by $\ln[\rho(\omega)]\sim\omega^4/T^2$ as advocated by Keyes [J. Chem. Phys. **101**, 5081 (1994)]. However, since in the relevant frequency range the two fits almost overlap, the numerical results obtained by Keyes, showing good agreement with the simulation results for self-diffusion in supercooled liquid argon, remain valid even though implications for the frequency dependence of the barrier height distribution change. We also explore other possibilities for extracting information from the INM analysis: (1) The density of ''zero force modes,'' defined as the distribution of normal modes found at the bottom or top of their parabolic potential surfaces, can be computed with no appreciable additional numerical effort. This distribution provides a better representation than the total density of modes for the normal mode distribution at well bottoms and at saddles, however, we find that it makes little difference in quantitative analysis. (2) We suggest that the ratio $\rho_u(\omega)/\rho_s(\omega)$ between the density of modes in the unstable and stable branches provide an estimate for the averaged barrier height distribution for large ω. Using this estimate in a transition state theory calculation of the average hopping time between locally stable liquid configurations and using the resulting time in a calculation of the self-diffusion coefficient yields a very good agreement with results of numerical simulation. © *1995 American Institute of Physics.*

I. INTRODUCTION

There has recently been a growing interest in applying normal mode analysis of instantaneous liquid configurations to the analysis of liquid state dynamics.[1–22] The applicability of the instantaneous normal mode (INM) picture (based on expanding the multidimensional potential surface up to quadratic terms in the deviation of the coordinates from the instantaneous initial configuration) is quite evident for the liquid dynamics at short times. This includes not only short time phenomena, but also transition and transport coefficients associated with correlation functions dominated by short time dynamics. A beautiful example has recently been given by the analysis of the short time dynamics of solvation by Stratt and Cho.[17]

While many dynamical processes are controlled by rates derived from relatively short lived time correlation functions, it has to be conceded that often in normal liquids the ''short times'' involved are not short enough for a straightforward normal mode evaluation of these rates. Consider for example the self diffusion coefficient $D=(1/3)\int\langle\mathbf{v}(0)\cdot\mathbf{v}(t)\rangle dt$, where $v(t)$ is the velocity. Its relatively small value in condensed systems results from cancellation of positive and negative contributions to the integrand at short times, making the long time behavior important in determining the overall value of D. It is remarkable that sometimes, in particular for strongly arrested motions, e.g., for dense enough monoatomic systems[5] or for the rotational motion in highly polar liquids such as water,[18] the Fourier transform of the density of *stable* modes yields a reasonable approximation for the velocity (or angular velocity) correlation function for relatively long times. (The Fourier transform of the total density of modes performs much more poorly because of the diverging time evolution of the imaginary frequency components.) Still, these approximations to the velocity correlation function are not good enough for evaluation of the self diffusion coefficient. Problem arise also in evaluating rates associated with finite frequency Fourier transforms of such time correlation functions because they are usually very sensitive to the detailed structure of these functions.

In spite of these shortcomings, Keyes and co-workers, in a series of recent papers[2–8] have shown that it is possible to use instantaneous normal mode analysis to obtain information about the self-diffusion coefficient of (supercooled) liquids. Keyes' ideas have developed substantially over the last few years, and in what follows we summarize them as presented recently by Keyes.[8] The starting point is Zwanzig's[1] expression for the self-diffusion coefficient, based on viewing the (monoatomic) liquid dynamics as a collection of damped harmonic motions

$$D=(kT/m)\int_0^\infty d\omega\ \rho_q(\omega)\frac{\tau_h}{1+\tau_h^2\omega^2}, \tag{1}$$

where m is the atomic mass, $\rho_q(\omega)$ is the density of harmonic modes associated with quenched (local minima) configurations and τ_h is their lifetime. Zwanzig's expression is in turn based on the idea of Stillinger and Weber[23] that the configuration space of the liquid may be viewed as a collection of ''inherent structures,'' local minima on the many body poten-

tial surface, about which the system executes two types of motions: small amplitude oscillations and (infrequent) transitions across potential barriers to other local minima. Zwanzig assumes that such transitions rearrange the equilibrium configuration in local subvolumes of the overall system (which consists of many such equivalent subvolumes), interrupt the oscillations of the harmonic modes associated with these subvolumes, and make the motions of these modes after the transition uncorrelated with their motions before it. τ_h is identified as the average waiting time for these transitions. It is important to realize that the idea of *subvolumes* affected by the transitions is associated with the realization that only modes of short enough wavelengths are affected by such transitions in a simple way; the lifetime of long wavelength hydrodynamic modes is controlled also by macroscopic conservation laws.

The important contribution of Keyes and co-workers is to provide estimates for $\rho(\omega)$ and τ_h to be used in Eq. (1). The most recent analysis of Keyes[8] is based on the following points:

(a) In Eq. (1), τ_h is taken as an average inverse hopping rate, independent of ω (the ''equivalent well model''[6]). Furthermore, it is assumed that $\tau_h(\omega) \gg 1$, leading to

$$D=(kT/m)\tau_h^{-1}\int_0^\infty d\omega\ \rho_q(\omega)\omega^{-2} \tag{2}$$

(b) The density $\rho_q(\omega)$ in Eq. (2) is approximated by the form

$$\rho_q(\omega)=(2\omega_s)^{-1}[1-\cos(\pi\omega/\omega_s)]; \quad 2\omega_s \geqslant \omega \geqslant 0, \tag{3}$$

where ω_s is peak frequency in the low temperature density of modes of the stable branch, $\rho_s(\omega)$. [For argon at reduced density $d=1$ (1.68 gr/cm^3) $\omega_S=12$ ($=5.5\cdot 10^{12}$ s^{-1}) estimated from the peak in $\rho_s(\omega)$ at $T=40$ K.)]

(c) The hopping times τ_h are associated with barrier crossing processes and are calculated using the transition rate theory expression rate $=(\omega_m/2\pi)\times[Q_B/Q_m]\exp(-E_B/kT)$, where ω_m is the characteristic well frequency, E_B is the characteristic barrier height and Q_B/Q_m is the ratio between partition functions associated with the subspace of stable modes in the barrier and well regions.[24]

(d) τ_h is estimated by averaging the barrier crossing rate over a distribution of saddle points according to

$$\tau_h^{-1}=\int_0^\infty d\omega(\omega_m/2\pi)[Q_B/Q_m]sn(\omega)e^{-\beta E_B(\omega)} \tag{4}$$

where $E_B(\omega)\equiv-\beta^{-1}\ln\langle e^{-\beta E_B}\rangle_\omega$ is the characteristic barrier height for barrier frequency ω; the average being over all barriers with curvature ω, s is the number of saddles connected to each well and $n(\omega)$ is the distribution of saddle frequencies, normalized to 1.

(e) The unstable branch of the normal mode density, $\langle\rho_u(\omega)\rangle$, is fitted to the functional form

$$\langle\rho_u(\omega)\rangle=a\omega\ \exp(-c\omega^4/T^2) \tag{5}$$

where the parameters a and c can be obtained from the fit. Using earlier theoretical arguments[6] yields an estimate for the characteristic barrier height at frequency ω

$$\langle e^{-\beta E_B}\rangle_\omega \approx \exp(-c\omega^4/T^2); \quad c\omega^4/T^2 \gg 1. \tag{6}$$

(f) The term $[Q_B/Q_m]sn(\omega)\exp(-\beta E_B(\omega))$ in Eq. (4) is associated with the averaged density of normal modes in the unstable (imaginary frequencies) branch, $\langle\rho_u(\omega)\rangle$, according to[8]

$$[Q_B/Q_m]sn(\omega)e^{-\beta E_B(\omega)}=\frac{\omega}{\omega_m}M\left(\frac{\alpha}{3z}-f_u\right)^{-1}\langle\rho_u(\omega)\rangle, \tag{7}$$

where M is the number of minima connected to each saddle, $\alpha/3z$ is the fraction of downward directions in a saddle and f_u is the fraction of unstable modes,

$$f_u=\int d\omega\langle\rho_u(\omega)\rangle. \tag{8}$$

(g) Equations (4), (5), and (7) then lead to

$$\tau_h^{-1}=\frac{M}{2\pi(\alpha/3z-f_u)}\int_0^\infty d\omega\ \omega\langle\rho_u(\omega)\rangle$$

$$=\frac{Ma}{2\pi(\alpha/3z-f_u)}\int_0^\infty d\omega\ \omega^2\ \exp(-c\omega^4/T^2). \tag{9}$$

Equations (2), (3), and (9) now provide a direct route from the averaged instantaneous normal modes density (both stable and unstable branches) to the self-diffusion coefficient. This analysis leads to $D/T=4.31\cdot 10^{-8}\,\mathrm{MT}^{3/2}$ (T in K and D in units of σ^2/t_u) and, with the simplest choice $M=2$ (i.e., one dimensional saddles connecting two neighbor minima) yields an excellent agreement with results of numerical simulations for supercooled liquid argon.[8]

The success of Keyes analysis is remarkable in that it demonstrates the feasibility of obtaining information pertinent to long time dynamics from data that appears to be relevant only to short times. Some assumptions and some intermediate results which underline Keyes analysis still appear questionable. Without underestimating the importance of Keyes ideas, we address in the present paper these points that we regard as weaker in the detailed analysis. The bottom line of our analysis is similar to that of Keyes, namely, the instantaneous normal modes of a liquid indeed contain data pertinent to long time dynamics. It appears however that the success in fitting the self-diffusion coefficient cannot in itself provide a confirmation to the detailed structure of this analysis.

In Sec. II, we re-examine the issue of barrier height distribution. Keyes[8] already pointed out that a simple geometrical argument[25] would suggest that the right-hand side of Eq. (6) should take the form $\exp(-c\omega^2/T)$ for large enough ω. Our numerical analysis of both normal and supercooled simulated liquid argon, lead us to indeed prefer this form for large enough ω. We show however that with parameters obtained from our numerical analysis the result (based on Keyes' procedure) for D remains essentially unchanged.

We also consider the origin of the stable and unstable normal mode distributions, $\rho_s(\omega)$ and $\rho_u(\omega)$. Keyes[8] assumes that these functions are dominated by wells, barriers and saddle points. In fact, Eqs. (4a) and (4b) in Ref. 8, which provide the basis for this analysis, rely heavily on this as-

sumption. However, there is no reason to underestimate the contribution of other points in configuration space, whose contribution to these distributions depend on the local anharmonicities.[26,27] Instead we suggest a procedure which bias the stable and unstable mode distributions in favor of the local vicinities of saddles and wells. As expected, the resulting distributions are significantly blueshifted relative to the normal, unbiased ones. It is significant and gratifying however that the resulting estimate for $\langle \exp(-\beta E_B)\rangle_\omega$ is only modestly affected by this new procedure.

In Sec. III, we consider another approach to the self-diffusion coefficient, based on the assumption that the ratio $\rho_u(\omega)/\rho_s(\omega)$ provides a measure of the relative barrier height between neighboring well and saddle characterized by a frequency ω. We show that this approach gives results in very close agreement to those obtained from numerical simulations for high density liquid argon. In Sec. IV, we summarize our findings and conclusions.

II. NORMAL MODE DISTRIBUTIONS

The numerical results presented in this paper are based on simulations of liquid argon as a Lennard-Jones fluid characterized by the well depth $\epsilon/k_B=119.8$ K and diameter $\sigma=3.405$ A. The same model fluid was used by Keyes and co-workers.[8] Using the argon mass m, the natural time unit for this system is $t_u\equiv[m\sigma^2/\epsilon]^{1/2}=2.18$ ps. All frequencies are expressed in units of t_u^{-1}. As usual all length coordinates are scaled by the atomic mass, $m^{1/2}l\rightarrow l$, so the force constants (eigenvalues of the Hessian matrix) satisfy $k=\omega^2$, where ω is the corresponding INM frequency. For reasons that become apparent below, we often deviate from the usual norm of plotting the density of normal modes as a function of ω, and plot it against k instead. We use ρ_ω and ρ_k to denote the corresponding mode densities. Note that $\rho_\omega(\omega)=2\omega\rho_k(|k|)$. In what follows, however, we sometimes omit the subscripts ω and k on ρ, when the meaning is apparent from the text.

The discussion in this paper focuses heavily on the normal modes distributions associated with the local minima and with the saddle points of the multidimensional potential surface of the liquid. Though these distributions can, in principle, be computed, the necessary numerical procedures are very time consuming especially with regards to saddle point locations. For this reason, Keyes and co-workers have focused on the density of modes obtained from sampling configurations from finite temperature trajectories. Here, we examine a simple way to weight the configuration sampled in favor of well bottoms and saddle points without almost any additional numerical effort. This is done by selecting only those frequencies associated with modes subjected to zero force in the sampled configuration. To this end suppose that for a given configuration the diagonalization of the Hessian leads to a set of N normal mode force constants $\{k_j\}$ and forces $\{f_j\}$. For an arbitrary small fraction $\delta\ll 1$ (we have used $\delta=0.017$), we select only a subset N_0 of the modes: those that satisfy $f_j<k_j\sigma\delta$. For δ small enough the number N_0/δ is independent of δ, and $N_0/(N\delta)$ measures the fraction of ''zero force modes'' in the given configuration. Thus the resulting subset contains only those modes which are found

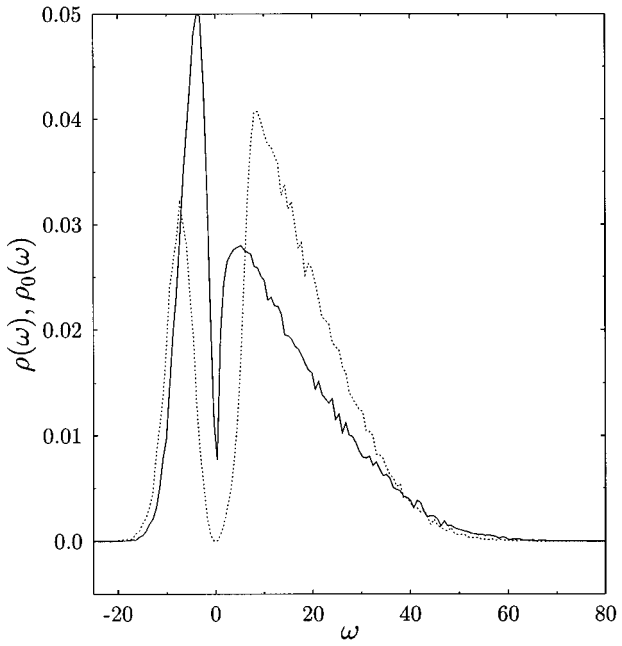

FIG. 1. The density of modes for liquid Ar at density $d=0.78$ (molecules per σ^3) and $T=150$ K. Full line—the total density $\rho(\omega)$. Dotted line—density of zero force modes, $\rho_0(\omega)$.

at the minimum (for stable modes) or maximum (for unstable modes) of the parabola on which they are defined. This set is used to construct the ''density of zero force modes,'' $\rho_0(\omega)$, in the same way that the overall set of modes, obtained without restrictions, is used to determine $\rho(\omega)$.

It is clear that $\rho_0(\omega)$ does not necessarily represent the saddles (for $\omega^2<0$) or wells (for $\omega^2>0$), because at such points *all* modes should be zero force modes. However, it is also clear that (a) $\rho_0(\omega)$ is a better representation for the density of modes associated with critical points (saddles and wells) on the potential surface, and (b) that if the size of the sample studies is larger than the size of the ''independent rearranging regions'' then real critical points of the sample are irrelevant.

Figures 1 and 2 show $\rho(\omega)$ and $\rho_0(\omega)$ for liquid argon at 150 K for two densities; $d=0.78$ and $d=1.0$ (molecules per σ^3). As in previous studies[2–8] the negative axis is used to display the branch of imaginary frequencies. These results and others shown below are based on simulations with 100 or 400 particles,[28] and are only very weakly sensitive to the system size. Note that both $\rho(\omega)$ and $\rho_0(\omega)$ are normalized to 1. We note that (a) Both real and imaginary branches of ρ_0 are shifted to higher frequencies relative to ρ. This is as expected from considering simple 1-dimensional pictures, since a substantial contribution to low frequencies arise from intermediate (between minima and maxima) configurations. (b) The dip about $\omega=0$ is much more pronounced in $\rho_0(\omega)$ than in $\rho(\omega)$, again as expected from similar reasoning. (c) Denoting the fraction of unstable modes $f_u=\int_{-\infty}^0 d\omega\,\rho(\omega)$ and $f_u^{(0)}=\int_{-\infty}^0 d\omega\,\rho_0(\omega)$, it is clear from Figs. 1 and 2 that $f_u>f_u^0$; again expected since ρ_0 samples a larger portion of phase space associated with real extrema in the potential surface, and these are weighted by the Boltzmann factor in favor of the local minima, i.e., real frequency extrema.

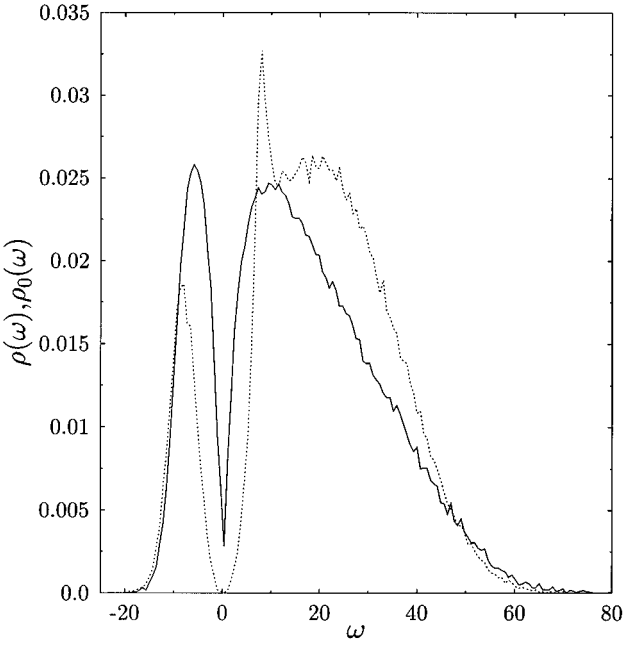

FIG. 2. Same as Fig. 1, for supercooled liquid Ar, $d=1$ and $T=150$ K.

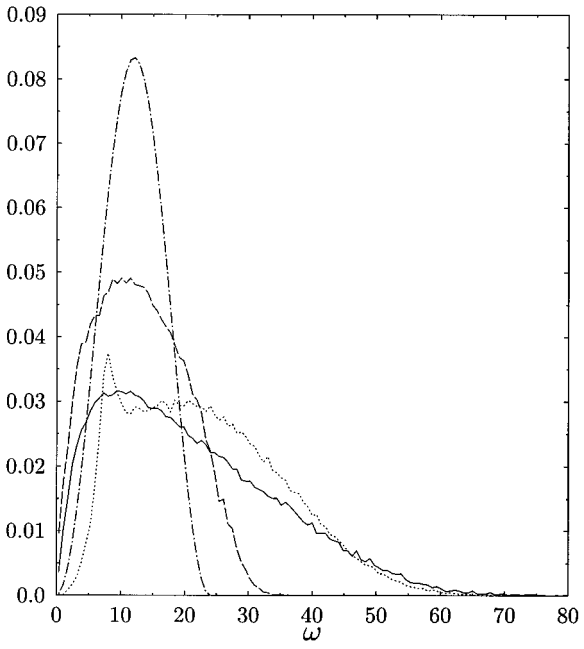

FIG. 3. Full line: The stable branch of the total density of modes, $\rho_s(\omega)$, of Fig. 2. Dotted line: The stable branch of the density of zero force modes, $\rho_{0s}(\omega)$, also shown in Fig. 2. Dashed line: The distribution of quenched, zero temperature modes, $\rho_q(\omega)$. Dashed–dotted line: The approximation (3) for $\rho_q(\omega)$. All distributions are for the dense, $d=1$, fluid. All are normalized to 1 in the domain $\omega=0\cdots\infty$.

These observations are all consistent with the expectation that $\rho_0(\omega)$ represent the density of modes at saddle points better than $\rho(\omega)$. It should be noted, however, that the substantial differences between these functions clearly indicate that anharmonicities in the potential surface contribute substantially to the detailed dependence of ρ on ω, and simple pictures that assign $\rho(\omega)$ to wells, barriers and saddles may fail in quantitative estimates.

In what follows we denote by $\rho_{0s}(\omega)$ and $\rho_{0u}(\omega)$ the stable and unstable branches, respectively, of $\rho_0(\omega)$. From the reasons just stated, $\rho_{0s}(\omega)$ itself cannot be regarded as a reliable approximation to the quenched density of modes, $\rho_0(\omega)$, since most of the stable modes that contribute to $\rho_{0s}(\omega)$ are associated with saddles and not with wells. A comparison of these three distributions for the $d=1$ liquid is shown in Fig. 3, which also depicts the approximation (3) used by Keyes for $\rho_q(\omega)$. The quenched density of modes used here is based on 50 configurations obtained from quenching 50 arbitrary initial configurations sampled from an equilibrium 150 K trajectory, using a conjugate gradient algorithm. The high frequency tails seen in $\rho(\omega)$ and (in a more pronounced way) in $\rho_{0s}(\omega)$ practically disappears in $\rho_q(\omega)$, which, in this respect, is represented relatively well by the approximation (3). This behavior can be rationalized by the fact that the saddles that contribute to the finite temperature $\rho_{0s}(\omega)$ are of higher energy, therefore sample strongly repulsive parts of the interatomic interaction not accessible at lower energies. These strong interactions at close atomic encounters are associated with higher frequencies, which is probably the cause for the finite temperature high frequency tails in $\rho_{0s}(\omega)$ and $\rho_s(\omega)$.

Next consider the detailed dependence of these distributions on $k=\omega^2$. We consider separately the stable and unstable branches, $\rho_s(|k|)$, $\rho_u(|k|)$, and similarly $\rho_{0s}(|k|)$, $\rho_{0u}(|k|)$. In constructing the corresponding histograms, windows of size $\Delta k=0.075(4k)^{2/3}$ were used.[29] This choice of collecting data yields relatively smooth curves even when $\rho(|k|)$ is as low as 10^{-8}. The resulting functions are shown in Figs. 4 and 5. Figures 4 display $\ln\rho_s(|k|)$ and $\ln\rho_u(|k|)$, respectively, for two liquid densities, $d=0.78$ and 1.0 as functions of k. Similar results for $\ln\rho_{0s}(|k|)$ and $\ln\rho_{0u}(|k|)$ are shown in Figs. 5. It is seen that for large $|k|$ these distributions are represented quite well by an exponential function, $\exp(-\alpha|k|)$, in contrast to the conclusion of Keyes who has fitted $\rho_u(|k|)$ to the form $\exp(-\alpha|k|^2)$.[30] In Fig. 6 we show again the data of Fig. 4(b) for the high density fluid, now plotted against k^2. In addition to our data, this figure also shows the fit by Keyes (results based on the dashed line of Fig. 11 in Ref. 8). It is seen that there is actually an excellent agreement between our results and Keyes' in the range where they can be compared, but based on our larger range of data we have reached a different conclusion.

Figure 7(a) shows $\ln\rho_u(|k|)$ vs k for several temperatures, $T=60$, 100, 150, and 200 K, for the $d=0.78$ fluid. The slopes of the large $|k|$ linear dependencies are plotted vs $1/T$ in the inset. Similar results for the $d=1$ fluid at $T=100$, 150, and 200 K are shown in Fig. 7(b). We conclude that for large $|k|$ $\rho_u(|k|)$ is represented well by the form

$$\rho_u(|k|)=A\ \exp(-B|k|/T), \tag{10}$$

i.e., $\rho_u(\omega)=2A\omega\ \exp(-B\omega^2/T)$. (We find $A=6.4\times10^{-3}$ and $B=3.7$ for $d=0.78$ and $A=6\times10^{-3}$, $B=5.0$ for $d=1$.) Thus like Keyes [Eq. (5) above], we find that $\rho_u(\omega)$ depends on T through the variable ω^2/T. We note that Keyes has pointed out that in going to low temperatures care has to be taken to include only supercooled fluid samples that did not become

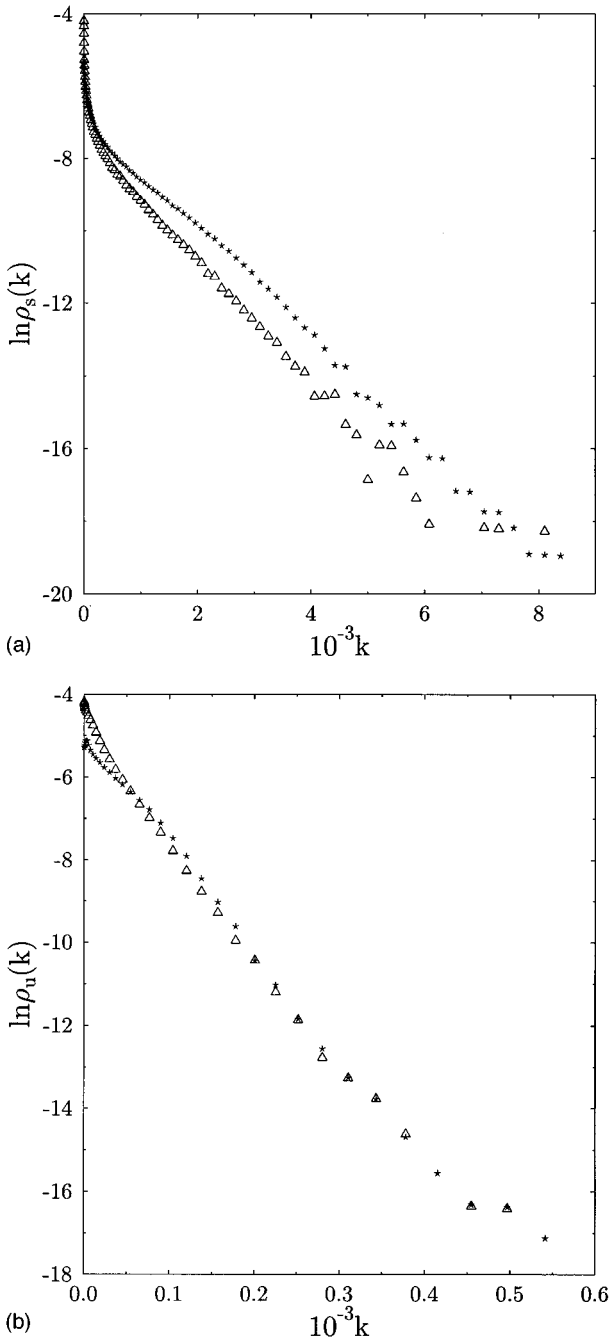

FIG. 4. (a) The distribution of eigenvalues in the stable mode branch: $\ln \rho_s(k)$ vs k. Triangles—$d=0.78$. Stars—$d=1.0$. (b) Same, for the distribution of eigenvalues in the unstable branch, $\rho_u(|k|)$.

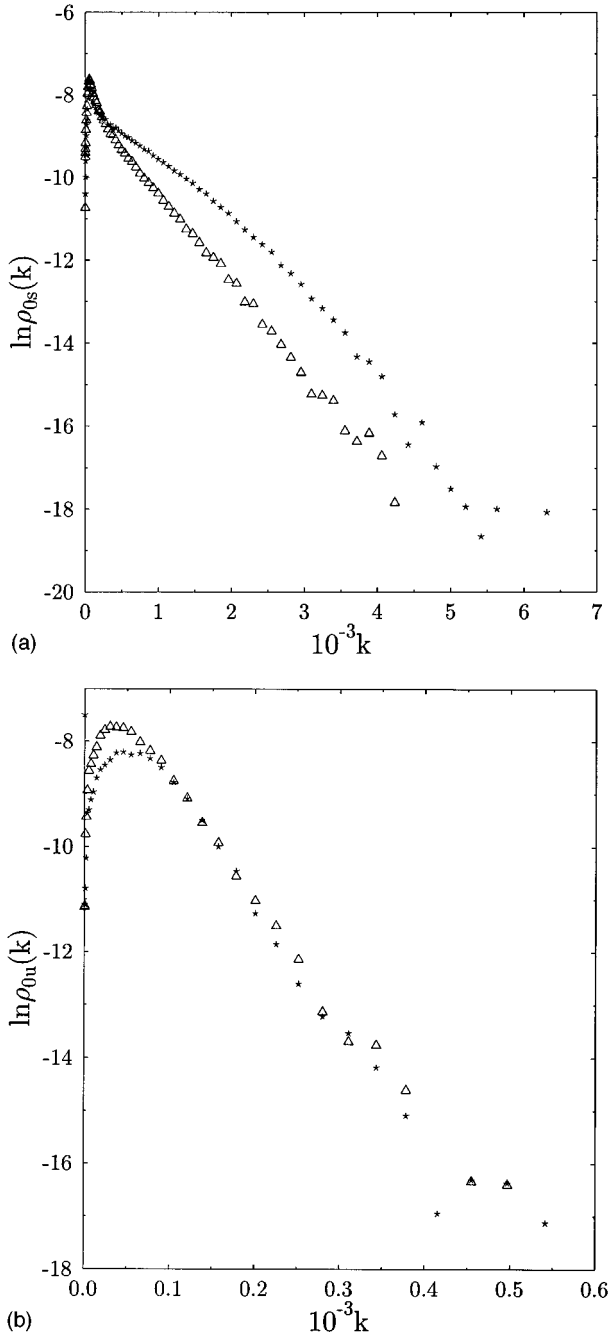

FIG. 5. Same as Fig. 4, for the distribution of zero force modes, $\rho_{0s}(k)$ and $\rho_{0u}(|k|)$.

solid glasses. This is not expected to create a problem for the lower density fluid, as we verified by monitoring the numerical self-diffusion coefficient, but it is the reason for limiting our studies of the high density fluid to $T \geqslant 100$ K.

Keyes[8] has used his results to predict the self-diffusion coefficient based on Eqs. (2), (3), and (9): $\rho_u(\omega)$ and f_u are directly obtained from the simulations and the parameter $\alpha/3z$ is estimated using the simulation data and the theory of Ref. 4(d). This resulted in $D/k_BT = 1.68 \cdot 10^5$ MT$^{3/2}$ cm^2/s (T in K), in close agreement with the simulation results if $M=2$ is chosen. This is an impressive success of the theory. However, since beyond the difference in the analytical form used to fit $\rho_u(\omega)$ [Eq. (10)] with $k=\omega^2$ instead of Eq. (5)] the numerical results are practically the same in the ω range that mostly contributes to the integral in Eq. (9), we would get very similar result for τ_h using $\rho_u(\omega) = 2A\omega \exp(-B\omega^2/T)$. Using this form and Eqs. (2), (3), and (9), with A, B, f_u and $\alpha/3z$ obtained from fitting our data for $\rho_u(\omega)$ we indeed get (using $M=2$) $D/k_BT = 1.42 \cdot 10^5$ MT$^{3/2}$ cm^2/s, in close agreement with Keyes. We have to conclude that the success in fitting the self-diffusion coefficient cannot in itself indicate the superiority of one of the forms used for $\rho_u(\omega)$ over the other.

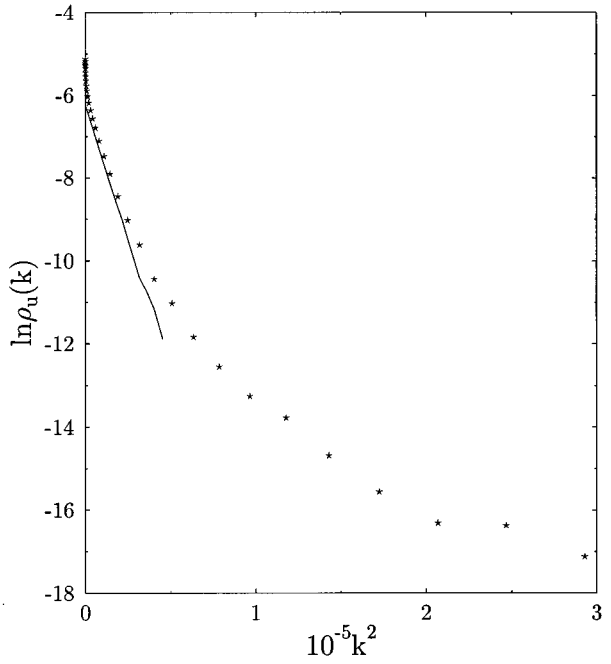

FIG. 6. Stars: Same results as in Fig. 4(b) (high density fluid, $d=1$) plotted against k^2. Full line: results from Ref. 8. (See the text.)

III. THE INDEPENDENT MODE MODEL

The data analysis in the previous section has followed that of Keyes,[8] which is based on the ''equivalent minima-fully collective model'' of Madan and Keyes.[6] In this section we follow a considerably more naive approach which seems to do at least as well. This approach is based on the following assumptions: (a) The escape from a local well (associated with an inherent liquid structure) is dominated by transitions through simple saddle points characterized by a single ''reaction coordinate,'' i.e., one unstable direction. (b) The corresponding neighboring well and barrier are associated with similar frequencies; in fact we assign the same ''reaction coordinate'' frequency ω (in absolute magnitude) to both. (c) The corresponding barrier height is correlated with ω. If the geometrical argument[25] that leads to $\epsilon(\omega)\sim|\omega|^2=|k|$ holds, the stable and unstable branches of the instantaneous normal mode distribution would satisfy

$$\frac{\rho_u(\omega)}{\rho_s(\omega)}=A\ \exp(-\epsilon(\omega)/k_BT);\quad \epsilon(\omega)\sim\omega^2(\omega\to\infty) \tag{12a}$$

or

$$\frac{\rho_u(|k|)}{\rho_s(|k|)}=A\ \exp(-\epsilon(|k|)/k_BT);\quad \epsilon(|k|)\sim|k|(|k|\to\infty). \tag{12b}$$

Figures 8–11 show that this expectation is indeed confirmed by the numerical experiment, provided that $k=\omega^2$ is large enough. Figure 8 show $\ln[\rho_u(|k|)/\rho_s(|k|)]$ plotted against k for the density $d=0.78$ at temperatures 60, 100, 150, and 200 K. Figure 9 shows similar results for $\ln[\rho_{0u}(|k|)/\rho_{0s}(|k|)]$. Linear dependence is seen for large k, and the corresponding slopes are displayed against $1/T$ in the insets. Similar results for the high density, $d=1$, fluid are shown in Figs. 10 and 11.

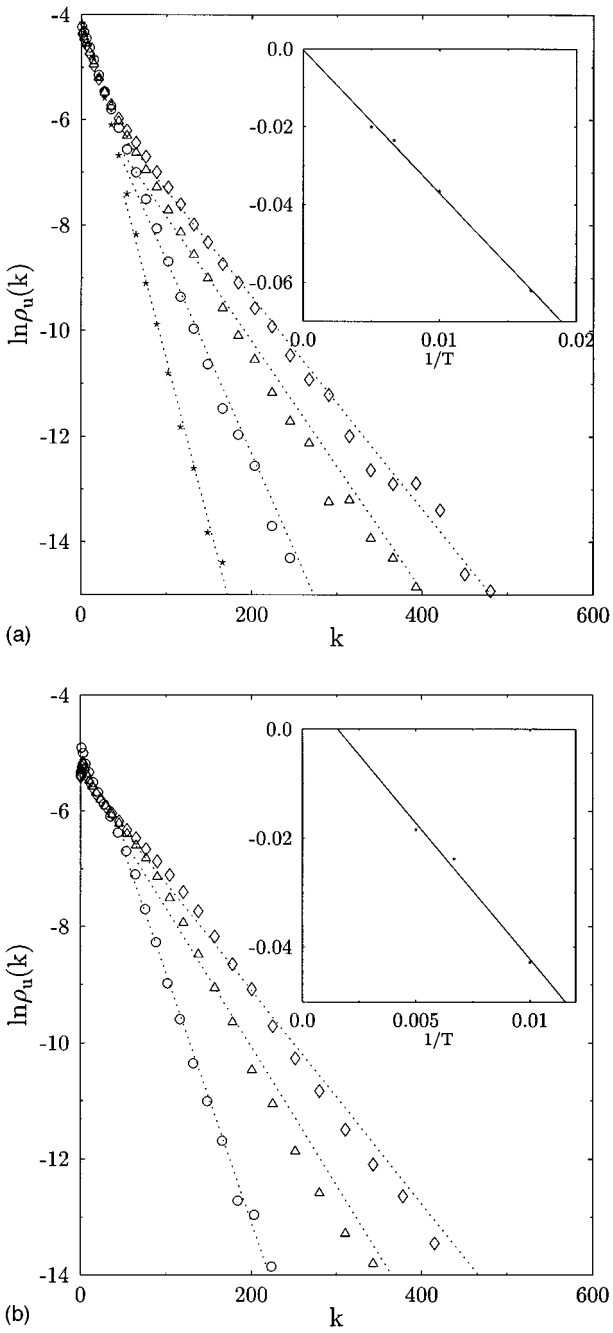

FIG. 7. (a) $\ln\rho_u(|k|)$ vs $|k|$ for the $d=0.78$ fluid at different temperatures: 60 K (stars), 100 K (circles), 150 K (triangles), and 200 K (diamonds). The inset shows the slopes of these lines as functions of inverse temperature. (b) Same as (a), for the $d=1$ fluid at $T=100$ K (circles), 150 K (triangles), and 200 K (diamonds).

It is seen that Eq. (12) is satisfied for both ρ and ρ_0. The (relatively small) quantitative difference observed between the behavior of ρ and ρ_0 indicates again that the total frequency distribution does not represent fully the distribution associated with wells, barriers and saddles. Table I summarizes the parameters obtained from these fits.

The function $\exp(-B|\omega|^2/k_B/T)$ should be interpreted as the result of the present theory for the average (over all barriers associated with frequency ω) of the Boltzmann factor $\exp(-E_B/k_BT)$, which in Keyes' theory is given by Eq. (6)

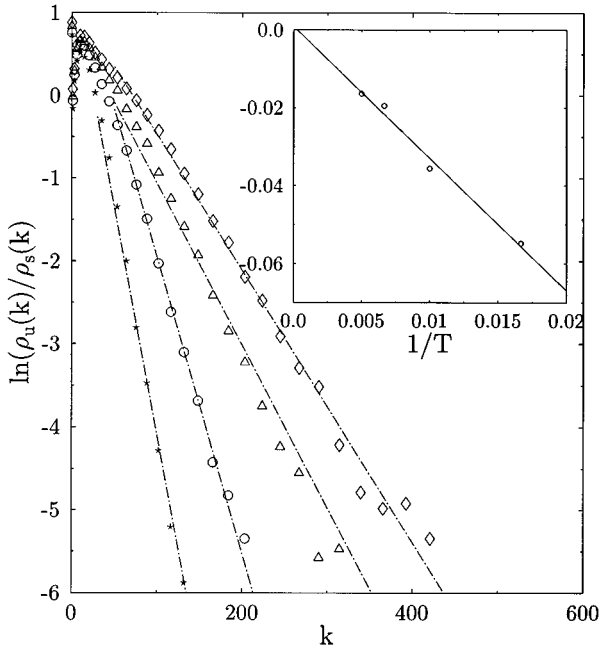

FIG. 8. $\ln[\rho_u(|k|)/\rho_s(|k|)]$ plotted against $|k|$ for the low density ($d=0.78$) fluid at $T=60$ K (stars), 100 K (circles), 150 K (triangles), and 200 K (diamonds). In the inset the slopes of these lines are plotted against $1/T$.

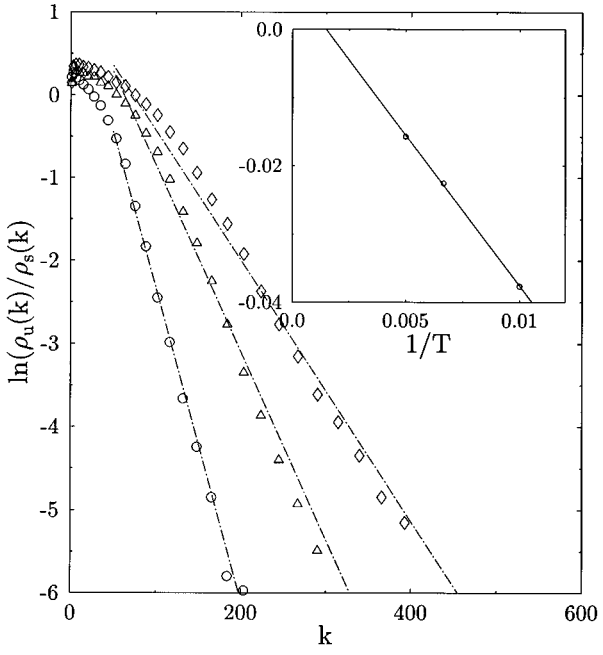

FIG. 10. Same as Fig. 8 for the high density ($d=1.0$) fluid at $T=100$ K (circles), 150 K (triangles), and 200 K (diamonds).

and for which we have already argued in the previous section that a quadratic frequency dependence of the barrier height provides a better representation than Eq. (6). The pre-exponential term A is, in the same average sense, a measure of the ratio of volumes associated with the non reactive modes in the corresponding saddle and well, the equivalent of the factor Q_B/Q_m in Eq. (4).

Carrying this picture to its naive conclusion, we now assign the lifetime τ_h in Eq. (1) to the inverse rate for crossing the barrier(s) connecting a local well to its neighbors, calculated from the transition state theory expression

$$\tau_h^{-1}=c\int_0^\infty d\omega\ \rho_q(\omega)\frac{\omega}{2\pi}A\ \exp[-\beta\epsilon(\omega)], \tag{13}$$

where the integral is an average over all the normal mode frequencies in the well and where the factor $A\ \exp(-\beta\epsilon(\omega))$

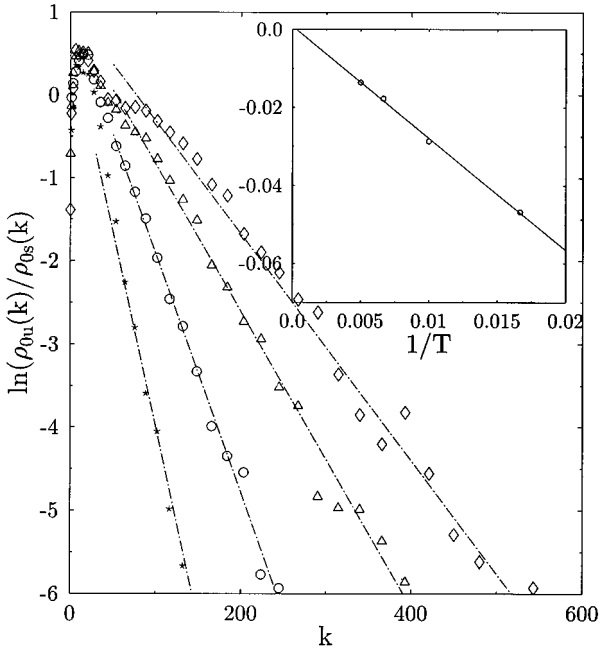

FIG. 9. Same as Fig. 8, for the ratios of zero force distributions obtained for the $d=0.78$ fluid: $\ln[\rho_{0u}(|k|)/\rho_{0s}(|k|)]$ plotted against $|k|$ at different temperatures with inset showing the slopes of the resulting linear dependencies plotted against $1/T$.

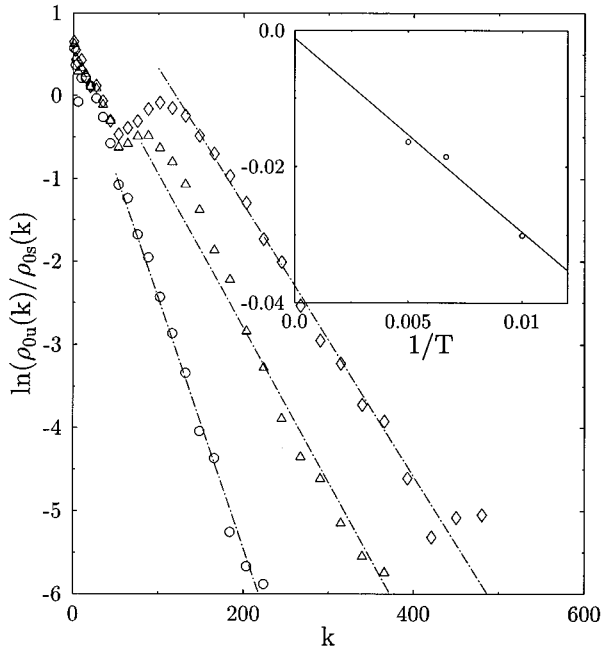

FIG. 11. Same as Fig. 9 for the high density, $d=1$. Mark notations are as in Fig. 10.

TABLE I. The parameters A and B obtained from fitting the ratio $\rho_u(|k|)/\rho_s(|k|)$ to the form (12b) with $\epsilon(|k|)/k_B = B|k|$ (in K).

Density/Distribution	A	B
0.78/Total	3.5	3.4
0.78/Zero forces	2.5	2.9
1.0/Total	3.8	4.4
1.0/Zero forces	3.2	2.8

is obtained from Eq. (12). In Eq. (13) we have allowed a constant fitting parameter c to allow for the fact that there may be more than one escape route out of a given well. It gives the same flexibility to Eq. (13) as given by the parameter M to Eq. (9) of Keyes' theory.

Figures 12 and 13 show the resulting diffusion coefficient, calculated from Eqs. (1) and (13), as a function of temperature for fluid density $d=1.0$. The simulation results from Keyes[8] are shown together with the best (integer) fit obtained by changing the multiplicative factor c in Eq. (13). Note that all calculations are done at constant volume. The full and dotted lines represent results obtained using Eq. (12) with the total density of modes ρ, and the density of zero force modes, ρ_0, respectively. In Fig. 12 $\rho_q(\omega)$ was represented by Eq. (3) with $\omega_s=12$, as in the applications done by Keyes. In this case the choice $c=3$ in Eq. (13) is seen to give a very reasonable fit. In Fig. 13, the numerically obtained quenched density of states shown in Fig. 3 (dashed line) was used. Here, good fits were obtained with $c=1$. We note that an attempt to repeat the same procedure for the normal fluid at $d=0.78$ did not succeed to reproduce the results of numerical simulations, and the best fits (which are still worse from those seen in Figs. 11 and 12) were obtained only for

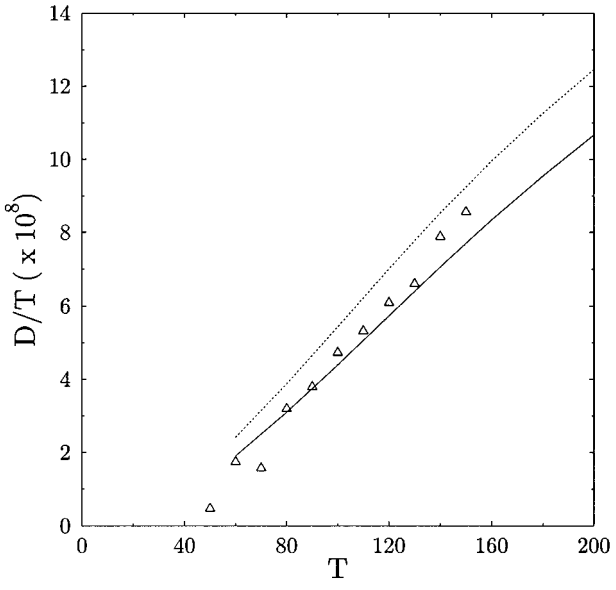

FIG. 12. D/T plotted against T for the high density, $d=1$, fluid. The triangles are Keyes' simulation results. Full line—results obtained using Eq. (12) for estimating $A\exp(-\epsilon/k_BT)$ in Eq. (13) using the total density of modes ρ and the multiplicative parameter $c=3$. Dotted line—results obtained similarly, using the density of zero force modes, $\rho_0(\omega)$, instead of $\rho(\omega)$. To produce the theoretical results the approximated quenched density of state, Eq. (3), has been used for $\rho_q(\omega)$ in Eq. (13).

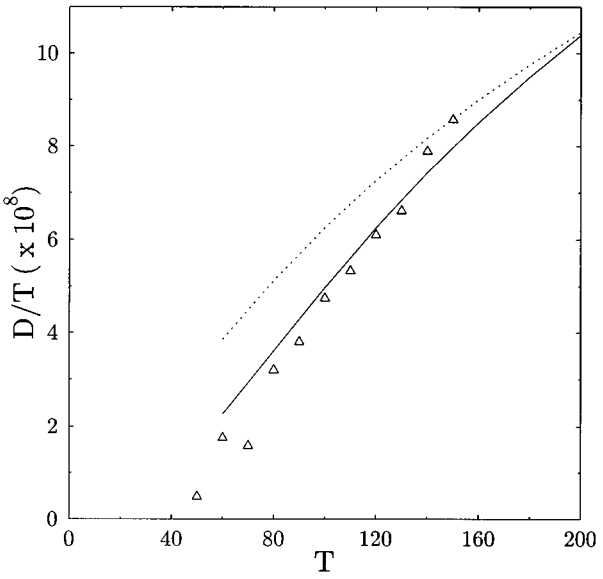

FIG. 13. Same as Fig. 12, except that the result of numerical quenching, the dashed line in Fig. 3, is used for $\rho_q(\omega)$ in Eq. (13), yielding $c=1$ as the parameter for best fit.

$c\cong 15$. This indicates, as emphasized by other workers[8,22,31] that the hopping mechanism for mass transport in liquids is relevant only at high densities, though perhaps not necessarily restricted to *supercooled* liquids.

IV. CONCLUSIONS

We have re-examined the application of instantaneous normal mode analysis to *long time* dynamics in liquids. Unlike the use of this concept to short time dynamics which is relatively straightforward, applications to long time dynamic processes such as self-diffusion rely on information about the distribution of barrier heights for hopping between inherent liquid structures (when this hopping dominates the dynamics). This course, taken before by Keyes,[8] was followed by us in the present work. Even though our conclusion concerning the barrier height distribution are different from Keyes', we have shown that in the range of numerically relevant data our results are very similar, providing support for the principal conclusions of Ref. 8. For the dependence of the average barrier height on the local reaction coordinate frequency we advocate $\langle E_B\rangle_\omega \sim \omega^2$, different from Keyes but more intuitively appealing.

We have also suggested another route for obtaining information on $\langle E_B\rangle_\omega$. This was based on the assumption that ratio $\rho_u(|\omega|)/\rho_s(|\omega|)$ between the density of modes in the unstable and stable branches is directly related to the relative barrier height associated with local wells and nearest neighbor saddles characterized by the frequency ω. We have shown that the barrier height distribution inferred from this approach, supplemented by a primitive form of transition state theory, provides a very reliable estimate for the self-diffusion coefficient of liquid argon at high density.

We should end with a word of caution: The success of our procedure, as well as that of Keyes,[8] indicates that the approaches taken contain much of the correct physics. How-

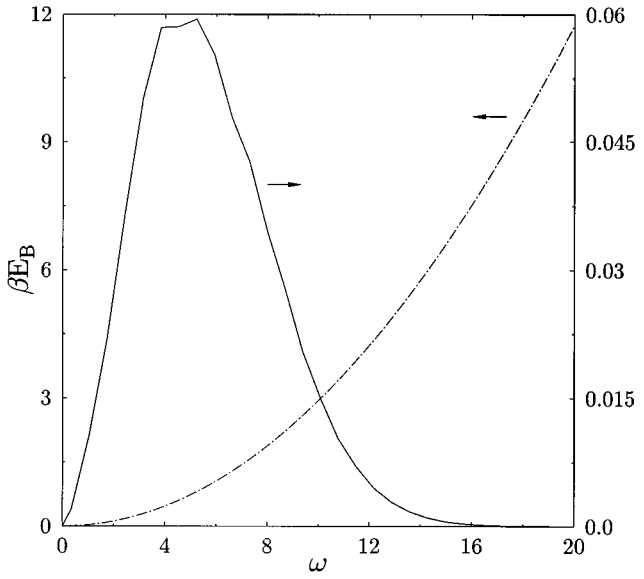

FIG. 14. $\epsilon(\omega)/k_BT$ (dashed–dotted line) and the full integrand of Eq. (13) (full line), plotted as a function of ω.

ever, the *quantitative* agreements seen in Figs. 12 and 13 should not be taken too seriously, as some assumptions were made with no real foundation. In particular it should be pointed out that the use of Eq. (13) in the present application is stretching this expression somewhat beyond the limits of its validity: This expression is valid for $\beta\epsilon(\omega)\gg 1$, however, this inequality is not satisfied in part of the ω region which contributes substantially to τ_h^{-1}. This is seen in Fig. 14, where both $\beta\epsilon(\omega)$ and the integrand in Eq. (13) is plotted as a function of ω. Here, the numerically quenched density $\rho_q(\omega)$ is used for the integrand of Eq. (13) and the total density of states is used in Eq. (12) to calculate $\beta\epsilon(\omega)$. [Very similar results are obtained when ρ_0 is used instead of ρ in Eq. (12).] It is seen that $\beta\epsilon \leqslant 1$ when the integrand attains its maximum as a function of ω. A similar problem exists also in Keyes' calculation. Nevertheless, the qualitative aspects of the present approach seem valid and it should be interesting to examine its applicability for more complicated liquids, in particular polar solvents.

ACKNOWLEDGMENTS

This research was supported in part by the U.S.—Israel Binational Science Foundation.

[1] Robert Zwanzig, J. Chem. Phys. **79**, 4507 (1983).
[2] G. Seeley and T. Keyes, J. Chem. Phys. **91**, 5581 (1989).
[3] B. Madan, T. Keyes, and G. Seeley, J. Chem. Phys. **92**, 7565 (1990).
[4] B. Madan, T. Keyes, and G. Seeley, J. Chem. Phys. **94**, 6762 (1991).
[5] G. Seeley, T. Keyes, and B. Madan, J. Phys. Chem. **96**, 4047 (1992).
[6] B. Madan and T. Keyes, J. Chem. Phys. **98**, 3342 (1993).
[7] P. Moore and T. Keyes, J. Chem. Phys. **100**, 6709 (1994).
[8] T. Keyes, J. Chem. Phys. **101**, 5081 (1994).
[9] I. Ohmine and H. Tanaka, Chem. Rev. **93**, 2545 (1993).
[10] J. D. Bauer and D. F. Calef, Chem. Phys. Lett. **187**, 391 (1991).
[11] B.-C. Xu and R. M. Stratt, J. Chem. Phys. **91**, 5613 (1989).
[12] B.-C. Xu and R. M. Stratt, J. Chem. Phys. **92**, 1923 (1990).
[13] K. Ganguly and R. M. Stratt, J. Chem. Phys. **97**, 1980 (1992).
[14] Z. Chen and R. M. Stratt, J. Chem. Phys. **97**, 5687 (1992).
[15] Z. Chen and R. M. Stratt, J. Chem. Phys. **97**, 5696 (1992).
[16] M. Buchner, B. M. Ladanyi, and R. M. Stratt, J. Chem. Phys. **97**, 8522 (1992).
[17] R. M. Stratt and M. Cho, J. Chem. Phys. **100**, 6700 (1994).
[18] M. Cho, G. R. Flemming, S. Saito, I. Ohmine, and R. M. Stratt, J. Chem. Phys. **100**, 6672 (1994).
[19] T.-M. Wu and R. F. Loring, J. Chem. Phys. **97**, 8568 (1992).
[20] T.-M. Wu and R. F. Loring, J. Chem. Phys. **99**, 8936 (1993).
[21] H. Stassen and Z. E. Gburski, Chem. Phys. Lett. **217**, 325 (1994).
[22] B. Bagchi, J. Chem. Phys. **101**, 9946 (1994).
[23] F. Stillinger and F. Weber, Phys. Rev. A **28**, 2408 (1983); J. Chem. Phys. **80**, 4434 (1984).
[24] Note that the definition of Q_B/Q_m here is different from v_B/v_m, the ratio of phase space volumes in the barrier and well regions of Ref. 8, by a factor of (in the harmonic approximation) ω_B/ω_m where ω_B is the barrier frequency.
[25] For a pair of neighboring barrier and well associated with the same frequency ω and located at a fixed distance from each other, the vertical energy difference scales as ω^2. This is expected to hold for modes of strong local character, i.e., large ω_0.
[26] Numerically we see a large accumulation of $k\sim 0$ modes in the $\rho(k)$ spectrum [see Fig. 4(a)], pointing to the importance of contributions not from saddles and not from well bottoms.
[27] We believe that the large estimate for the parameter $\alpha/3z\sim 0.43$ (α is the number of atoms in the independent rearranging regions) results from this assumption. For a modest $z=6$ this would imply $\alpha=8$. This implies that the dimension of the saddle—the number of downward directions and z is the typical saddle has 8 reactive directions, while the fit to the diffusion constant uses one such direction.
[28] Ensembles of 2000 configurations and of 50 configurations were used for the 100 particle system and the 400 particle system, respectively.
[29] This is done by defining $k=x^3/4$ and using windows of constant width in x. The natural alternative, to use windows of fixed width in ω, i.e., $\delta k=2k^{1/2}\delta\omega$, with $\delta\omega=0.1$ was used to construct the histograms for $\rho(\omega)$ and $\rho_0(\omega)$ in Figs. 1 and 2. Making the same choice here yields very similar results with somewhat bigger scatter of data in the large $|k|$ range.
[30] A possible exception is $\ln\rho_{0s}(|k|)$ in the high density fluid, which we found to be represented almost as well by both forms, i.e., the best fit would be to $\exp(-\alpha k^x)$ with $1<x<2$.
[31] U. Mohanty, Phys. Rev. A **32**, 3055 (1985).